ELSEVIER

International Journal of Heat and Fluid Flow 19 (1998) 209–222

International Journal of HEAT AND FLUID FLOW

A new low-Reynolds-number nonlinear two-equation turbulence model for complex flows

D.D. Apsley, M.A. Leschziner

Department of Mechanical Engineering, UMIST, PO Box 88, Manchester, M60 1QD, UK

Received 23 January 1997; accepted 13 August 1997

Abstract

A new nonlinear, low-Reynolds-number k–ε turbulence model is proposed. The stress–strain relationship is formed by successive iterative approximations to an algebraic Reynolds-stress model. Truncation of the process at the third iteration yields an explicit expression for the Reynolds stresses that is cubic in the mean velocity gradients and circumvents the singular behaviour that afflicts the exact solution at large strains. Free coefficients are calibrated – as functions of y^* – by reference to direct numerical simulation (DNS) data for a channel flow. By using the nonlinear stress–strain relationship, the sublayer behaviour of all turbulent stresses is reproduced. The extension to nonequilibrium conditions is achieved by sensitising the model coefficients to strain and vorticity invariants on the basis of formal relations derived from the algebraic Reynolds-stress model. The new model has been applied to a number of complex two dimensional (2-D) flows, and its performance is compared to that of other linear and nonlinear eddy-viscosity closures.

Keywords: Turbulence modelling; Computational fluid dynamics; Nonlinear k–ε model

Notation

$\mathbf{a} = (a_{ij})$	anisotropy tensor, Eq. (1)
C	coefficient of linear term in nonlinear eddy-viscosity model (NLEVM)
C_μ	coefficient in standard k–ε model
$C_{\varepsilon 1},\ C_{\varepsilon 2}$	coefficients in ε equation
D	damping factor in ε equation
$\mathrm{D}/\mathrm{D}t = (\partial/\partial t) + U_j(\partial/\partial x_j)$	derivative following the mean flow
f_μ	damping factor in low Reynolds-number eddy-viscosity formula
f_P	nonequilibrium factor in NLEVM coefficients
$\mathbf{I}$	identity matrix
k	turbulent kinetic energy
$l_\varepsilon = k^{3/2}/\varepsilon$	dissipation length
$P = \frac{1}{2}P_{kk}$	rate of production of turbulent kinetic energy
P_{ij}	rate of production of $\overline{u_i u_j}$
q_1, q_2, q_3	coefficients of quadratic terms in NLEVM
$R_\mathrm{t} = k^2/\nu\varepsilon$	turbulent Reynolds number
Re	Reynolds number
$\mathbf{s} = (s_{ij})$	dimensionless mean-strain tensor, Eq. (2)
$\overline{s}$	dimensionless mean-strain invariant, Eq. (5)
$U_i = (U, V, W)$	mean-velocity components
$u_i = (u, v, w)$	turbulent-velocity components
$x_i = (x, y, z)$	cartesian coordinates
y_n	wall-normal distance
$y^* = y_n k^{1/2}/\nu$	dimensionless wall-normal distance
α, β, γ	coefficients in algebraic Reynolds-stress model, Eq. (13)
$\overline{\alpha}, \overline{\beta}, \overline{\gamma}$	values of $\alpha\sigma,\ \beta\sigma,\ \gamma\sigma$ in log layer, Eq. (26)
$\gamma_1, \gamma_2, \gamma_3, \gamma_4$	coefficients of cubic terms in NLEVM
ε	rate of dissipation of turbulent kinetic energy
ε_w	function with theoretical near-wall asymptotic behaviour of ε
ν	kinematic molecular viscosity
ν_t	eddy viscosity
$\sigma = (k/\varepsilon)\sqrt{(\partial U_i/\partial x_j)^2}$	dimensionless shear parameter
$\sigma_k, \sigma_\varepsilon$	turbulent Prandtl numbers in k and ε equations, respectively
Φ_{ij}	pressure–strain correlation
$\boldsymbol{\omega} = (\omega_{ij})$	dimensionless mean-vorticity tensor, Eq. (2)
$\overline{\omega}$	dimensionless vorticity invariant, Eq. (5)

0142-727X/98/$19.00
PII: S0142-727X(97)10007-8

Superscript	
$\sim$	curve fit (as function of y^*) to DNS data for channel flow
Subscript	
∞	log-law region (mathematically, $y^* \to \infty$)
For a general matrix	
m	$\{\mathbf{m}\}$ denotes the trace m_{kk}, $m_2 = \{\mathbf{m}^2\}$, $m_3 = \{\mathbf{m}^3\}$, etc.

1. Introduction

First-order-closure models of turbulence assume an explicit algebraic relationship between Reynolds stresses and mean-velocity gradients. The popularity of linear (Boussinesq) eddy-viscosity models (EVMs) is based upon a theoretical justification in simple shear flows, their success in attached, fully-turbulent boundary layers subject to weak pressure gradients, and the ease of their incorporation into existing Navier–Stokes codes. Their range of applicability is broadened by formulating the eddy viscosity, ν_t, in terms of two scale-determining transport variables, such as k and ε (Launder and Spalding, 1974) or k and ω (Wilcox, 1994). Such models work well in two dimensional (2-D) thin shear flows, where only one Reynolds stress component is dynamically significant. However, practical engineering flows exhibit complex mean strain associated, for example, with streamwise pressure gradients, separation, impingement, streamline curvature, and swirl. These features are, in turn, sensitive to the turbulence structure – especially anisotropy – as well as history effects.

The minimum level of turbulence closure capable of resolving both anisotropy and history effects with any degree of rigour is *second-moment closure*, wherein transport equations are solved for each individual stress component. However, for general three dimensional (3-D) calculations, such *differential stress models* (DSMs) are costly, often unstable, and contain many terms that require modelling. A promising alternative, which has received increasing attention in the past few years, is to develop *nonlinear eddy-viscosity models* (NLEVMs), with the aim of accounting correctly for the effects of complex strain (Speziale, 1987, Shih et al., 1993, Gatski and Speziable, 1993, Craft et al., 1997).

Near solid boundaries, the use of log-law-based wall functions, which assume near-equilibrium turbulence and limit grid refinement by requiring the near-wall node to lie in the fully-turbulent region, is generally regarded as inferior to a direct integration through the viscous sublayer. In the k–ε framework, the latter requires two modifications – a viscosity-dependent factor f_μ in the eddy viscosity, representing both true viscous damping and preferential damping of wall-normal velocity fluctuations, and a modification of the dissipation-rate equation, so as to return the correct asymptotic behaviour near the wall. Viscous damping factors are typically functions of $y^* = y_n k^{1/2}/\nu$ (where y_n is the wall-normal distance) and/or the turbulent Reynolds number $R_t = k^2/\nu\varepsilon$. In constructing a *low*-Re NLEVM, a common approach is simply to multiply the nonlinear terms by the factor f_μ. However, this ignores the different behaviour of individual stresses: for example, $\overline{v^2}/k$ vanishes as the wall is approached; whereas $\overline{u^2}/k$ and $\overline{w^2}/k$ tend to nonzero values. This paper describes an alternative model that respects this distinct behaviour.

The remainder of this paper starts with, in Section 2, a general analysis of nonlinear stress–strain relationships, demonstrating the effects of the nonlinear terms. A new cubic low-Re k–ε model is then derived in Section 3. In Section 4, the application of NLEVMs to 2-D separated flows around an aerofoil, in an asymmetric diffuser, and behind a backward-facing step is reported and discussed. This is followed by general conclusions in Section 5.

2. The nonlinear stress–strain relationship

2.1. Foundations

In what follows, cartesian tensors of rank 2 are boldface (e.g., **T**), and their components are italicised (e.g., T_{ij}). Contracted products are written as for matrix multiplication: $(\mathbf{ST})_{ij} \equiv S_{ik}T_{kj}$. The *trace*, T_{kk}, of a tensor is denoted by $\{\mathbf{T}\}$, and the second and higher invariants by $T_2 \equiv \{\mathbf{T}^2\} \equiv T_{ij}T_{ji}$, $T_3 \equiv \{\mathbf{T}^3\} \equiv T_{ij}T_{jk}T_{ki}$, etc. Components of mean velocity are denoted by U_i and turbulent fluctuations by u_i. The turbulent kinetic energy is $k \equiv \frac{1}{2}\overline{u_i u_i}$, and its production and dissipation rates are P and ε, respectively. The anisotropy tensor **a** is defined by

$$a_{ij} = \frac{\overline{u_i u_j}}{k} - \frac{2}{3}\delta_{ij} \tag{1}$$

and the dimensionless mean strain and vorticity tensors, **s** and **ω** by

$$s_{ij} = \frac{1}{2}\left(\frac{\partial U_i}{\partial x_j} + \frac{\partial U_j}{\partial x_i}\right)\frac{k}{\varepsilon}, \qquad \omega_{ij} = \frac{1}{2}\left(\frac{\partial U_i}{\partial x_j} - \frac{\partial U_j}{\partial x_i}\right)\frac{k}{\varepsilon}. \tag{2}$$

The foundations of nonlinear eddy-viscosity modelling were laid by Pope (1975), who proposed a general constitutive relationship between Reynolds stresses and mean strain in incompressible flow:

$$\mathbf{a} = \sum_{\lambda=1}^{10} G_\lambda(\eta_1, \ldots, \eta_5)\mathbf{T}_\lambda(\mathbf{s}, \boldsymbol{\omega}). \tag{3}$$

The $\mathbf{T}_\lambda$ are linearly-independent, symmetric, traceless tensors that are coordinate-invariant, homogeneous tensor combinations of **s** and **ω**, while the η_r are invariants of the form $\{\mathbf{s}^\alpha\boldsymbol{\omega}^\beta\mathbf{s}^\gamma\boldsymbol{\omega}^\delta\ldots\}$. The finite number of invariants and tensorially independent products of **s** and **ω** are a consequence of the Cayley–Hamilton theorem of matrix algebra.

It is shown later that sensitivity to normal-stress anisotropy and mean-streamline curvature can be achieved by a simpler *cubic* stress–strain relationship, which can be written in the canonical form

$$\begin{aligned}\mathbf{a} = {} & -2C\mathbf{s} + q_1\left(\mathbf{s}^2 - \frac{1}{3}s_2\mathbf{I}\right) + q_2(\boldsymbol{\omega}\mathbf{s} - \mathbf{s}\boldsymbol{\omega}) + q_3\left(\boldsymbol{\omega}^2 - \frac{1}{3}\omega_2\mathbf{I}\right) \\ & - \gamma_1 s_2\mathbf{s} - \gamma_2\omega_2\mathbf{s} - \gamma_3\left(\boldsymbol{\omega}^2\mathbf{s} + \mathbf{s}\boldsymbol{\omega}^2 - \omega_2\mathbf{s} - \frac{2}{3}\{\boldsymbol{\omega}\mathbf{s}\boldsymbol{\omega}\}\mathbf{I}\right) - \gamma_4(\boldsymbol{\omega}\mathbf{s}^2 \\ & - \mathbf{s}^2\boldsymbol{\omega}).\end{aligned} \tag{4}$$

The grouping of cubic terms–for example, the appearance of $\omega_2\mathbf{s}$ in two separate elements–is for convenience: the last two terms vanish identically in 2-D incompressible flow. Note that $s_2 \equiv \overline{s}^2/2$, $\omega_2 = -\overline{\omega}^2/2$ where

$$\overline{s} = \sqrt{2s_{ij}s_{ij}}, \qquad \overline{\omega} = \sqrt{2\omega_{ij}\omega_{ij}} \tag{5}$$

are the dimensionless strain and vorticity invariants, respectively.

In the first line of Eq. (4) the conventional linear k–ε model is recovered with $C = C_\mu$. The q_i-related terms are quadratic in mean-velocity gradients. Examples of nonlinear models terminated at this level are the material-frame-indifferent model of

Speziale (1987), the renormalisation-group model of Rubinstein and Barton (1990), and the realisable models of Shih et al. (1993, 1995). The γ_i-related terms are cubic in the mean-velocity gradients. Examples include the models of Lien et al. (1996) – strictly a low-Re, cubic extension of the model of Shih et al. (1993) – and Craft et al. (1997). In the latter, the coefficients are further sensitised to the anisotropy invariant A_2, for which a third transport equation (derived from a DSM) may be solved.

The addition of quadratic terms allows normal-stress anisotropy to be resolved, while cubic terms introduce sensitivity to mean streamline curvature and swirl. There is some ambiguity in referring to the (γ_1, γ_2) terms as cubic, because they are tensorially linear, i.e., proportional to **s**, and could be combined with the linear term. However, insofar as their *role* is distinct – in promoting sensitivity to curvature – it is convenient to regard them as separate entities.

The succeeding subsections highlight certain consequences of the nonlinear stress–strain relationship (4) for specific types of strain. Sections 2.3 and 2.4, in particular, relate to features that can be resolved only by including the nonlinear terms.

2.2. Two-dimensional incompressible flow

In any 2-D incompressible flow, it can be shown readily that the cubic terms associated with γ_3 and γ_4 vanish and that the quadratic terms make no explicit contribution to the production of turbulent kinetic energy by mean shear:

$$P \equiv -\overline{u_i u_j}\frac{\partial U_i}{\partial x_j} = \varepsilon\{-\mathbf{as}\}. \tag{6}$$

For a linear eddy-viscosity model, $P/\varepsilon = C_\mu \bar{s}^2$ and the production of k is unconditionally positive. However, this is no longer true for the general nonlinear model.

2.3. Normal-stress anisotropy in simple shear

When $\partial U/\partial y$ is the only nonzero mean-velocity derivative, the canonical form Eq. (4) gives

$$\begin{aligned} a_{11} &\equiv \overline{u^2}/k - 2/3 = (q_1 + 6q_2 - q_3)\sigma^2/12, \\ a_{22} &\equiv \overline{v^2}/k - 2/3 = (q_1 - 6q_2 - q_3)\sigma^2/12, \\ a_{33} &\equiv \overline{w^2}/k - 2/3 = -(q_1 - q_3)\sigma^2/6, \\ a_{12} &\equiv \overline{uv}/k = -C\sigma - (\gamma_1 - \gamma_2)\sigma^3/4, \end{aligned} \tag{7}$$

where $\sigma = (k/\varepsilon)\partial U/\partial y$. From this, it is seen that, in simple shear, the quadratic terms are responsible for normal-stress anisotropy, because, without them, the normal stresses, $\overline{u_\alpha^2}$ would all be equal to $2k/3$, in contradiction to experiment. Speziale (1987) demonstrates that normal-stress anisotropy is necessary for the development of secondary flows in noncircular ducts.

It is common, although by no means essential, to take $\gamma_1 = \gamma_2$, in order that the cubic terms have no effect in simple shear, or, as in the model presented in Section 3, to relate them to the linear and quadratic coefficients. This, together with the observation that solid-body rotation should have no effect on the stress field, so that $q_3 = 0$, yields, in simple shear, three equations for the unknown coefficients, C, q_1 and q_2, in terms of the three independent anisotropy components. In Section 3, Eq. (7) is used to calibrate a low-Re nonlinear model.

In general, the weak effect of the quadratic terms on the shear stress, the fact that in 2-D mean flow they have no effect on the production of k, and the need to incorporate the important effect of mean-streamline curvature, motivates the addition of cubic terms. The effect of these terms in curved shear flow is considered below.

2.4. Effects of curvature

The stabilising/destabilising effects of mean-streamline curvature can be demonstrated by considering the production terms in the Reynolds-stress equations. At any particular point of interest, consider a cartesian coordinate system whose x-axis is *locally* aligned with the flow. Shear is then manifested by the nonvanishing of $\partial U/\partial y$ and curvature by the nonvanishing of $\partial V/\partial x$. (In streamline coordinates, $\partial V/\partial x = -\kappa U_s$, where the *curvature* κ – the reciprocal of the radius of curvature – and the unit normal vector $\vec{e}_n$, which determines the y-direction, are defined by $\partial \vec{e}_s/\partial s = -\kappa \vec{e}_n$, with $\vec{e}_s$, a unit vector in the direction of the mean flow.) Shear makes a contribution $-2\overline{uv}(\partial U/\partial y)$ to the Reynolds-stress production term P_{11}, while curvature makes a contribution $-2\overline{uv}(\partial V/\partial x)$ to P_{22}. Assuming $\overline{uv}$ to have the sign of $\partial U/\partial y$, then, for a curved shear flow,

$$\frac{P_{22}}{\varepsilon} = \frac{-\overline{uv}}{\varepsilon}\frac{\partial V}{\partial x} \approx C_\mu\left(\frac{k}{\varepsilon}\right)^2 \frac{\partial U}{\partial y}\frac{\partial V}{\partial x} = \frac{C_\mu}{4}(\bar{s}^2 - \bar{\omega}^2). \tag{8}$$

Thus, the sign and magnitude of the curvature effect are determined by the parameter $\bar{s}^2 - \bar{\omega}^2 = 2(s_2 + \omega_2)$, with "stabilising" curvature, i.e., a tendency to reduce turbulent energy, present when $\bar{s}^2 - \bar{\omega}^2 < 0$ and typically associated with convex surfaces (Fig. 1), where the velocity increases away from the centre of curvature.

The effect of curvature may be *mimicked* by the (γ_1, γ_2) cubic terms in the nonlinear stress–strain relationship (4). These cubic terms are proportional to the linear term and simply change the effective C_μ:

$$C_\mu = C + \frac{1}{4}(\gamma_1 \bar{s}^2 - \gamma_2 \bar{\omega}^2). \tag{9}$$

Thus, as anticipated, the effect of curvature is determined by the parameter $\bar{s}^2 - \bar{\omega}^2$, and has the correct sign, provided γ_1 and γ_2 are positive. A similar analysis can be used to link the γ_4-related term to swirl (Craft et al., 1997).

2.5. Coefficients of existing nonlinear k–ε models

The coefficients of some quadratic and cubic NLEVMs that have been tested by the present authors are listed in Table 1. With the exception of the model of Lien et al. (1996), these are high-Re forms, and viscous damping factors are necessary to apply them in the near-wall sublayer. Speziale's model has, in its original form, terms involving $DS_{ij}Dt$, as part of the "Oldroyd derivative": the present authors have found it impossible to obtain numerically-stable solutions with these terms included and have, therefore, been obliged to neglect them. In Shih et al.'s model, consideration of flows for which the rotational strain $\bar{\omega}$ is much larger than the irrotational strain $\bar{s}$ shows that the model does not enforce positive normal stresses, as the authors apparently intended.

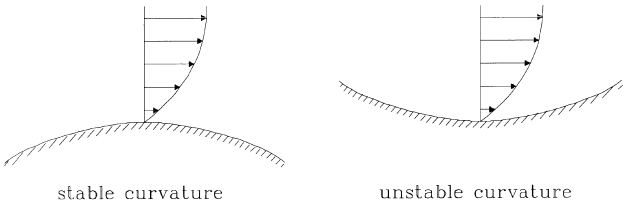

Fig. 1. Stabilising and destabilising mean-streamline curvature in a turbulent shear flow.

Table 1
Coefficients of various nonlinear eddy-viscosity models

Model	C	q_1	q_2	q_3	γ_1	γ_2	γ_3	γ_4
Speziale (1987)	0.09	0.054	q_1	0	0	0	0	0
Rubinstein and Barton (1990)	0.085	0.230	0.047	0.189	0	0	0	0
Shih et al. (1993)–SZL	$\frac{2/3}{(1.25+\tilde{S}+0.9\tilde{\omega})}$	$\frac{3}{1000+\tilde{S}^3}$	$5q_1$	$-\frac{19}{3}q_1$	0	0	0	0
Lien et al. (1996)	$f_\mu C_{\mathrm{SZL}}$	$f_\mu q_{1,\mathrm{SZL}}$	$5q_1$	$-\frac{19}{3}q_1$	$16f_\mu C_{\mathrm{SZL}}^3$	γ_1	0	$-5\gamma_1$

3. A new low-Re nonlinear eddy-viscosity model

3.1. Motivation

In Section 2 it was shown that the addition of nonlinear terms to the stress–strain constitutive relationship can mimic the response of turbulence to certain complex strains, whilst the model remains within a one- or two-equation framework. To account for normal-stress anisotropy and mean-streamline curvature, the stress–strain relationship must be at least cubic in products of the mean-velocity gradients. Because complex strains often coincide with complex boundaries, the inadequacies of wall functions motivate the search for a model capable of integrating through the viscous sublayer. To resolve the different behaviour of individual stresses, the coefficients of the various nonlinear terms must have different low-Re damping functions.

The new low-Re model is cubic in products of the mean-velocity gradients and is based upon three primary elements.

1. A formal nonlinear stress–strain relationship is obtained by successive iterative approximations to the solution of an algebraic Reynolds-stress model.
2. The free coefficients are calibrated (as functions of y^*) against DNS data for plane channel flow, by expressing them in terms of the anisotropy components a_{ij} and dimensionless shear σ.
3. Coefficients are extended to nonequilibrium conditions – by consideration of their P/ε dependence – in a manner that ensures that anisotropy components are bounded.

As a subsidiary element, viscous terms deduced from DNS data appear in the dissipation-rate equation. Alternatively, the dissipation length scale may be specified algebraically.

3.2. Simplification of an algebraic Reynolds-stress model

The idea of generating a NLEVM from an implicit, algebraic Reynolds-stress model – itself derived by simplification of a differential stress model – is not novel. It was first described by Pope (1975) and subsequently developed by Gatski and Speziable (1993). It can be shown that the Cayley–Hamilton theorem ("a matrix satisfies its own characteristic equation") implies that there are only a finite number of independent products of powers of $\mathbf{s}$ and $\boldsymbol{\omega}$ and that an algebraic system for stresses based on a linear model for the pressure–strain interaction could be solved *exactly*, yielding quadratic and quintic NLEVMs in 2- and 3-D flows, respectively. (According to Gatski and Speziable, the coefficient of the quintic term turns out to be zero, so that their NLEVM is actually quartic.) An unattractive feature of the exact solution is that it can become singular for large strains, leading Gatski and Speziable to "regularise" their stress–strain relationship by using nonsingular Padé approximants for nonequilibrium flows.

The present approach does not attempt to solve the algebraic system exactly, but generates the terms of successive order in a NLEVM by repeated iterative approximation. This has several advantages: it is relatively simple mathematically, while still retaining all the qualitative effects of anisotropy; it yields no singularities for large strains; and it could, in principle, be applied in conjunction with nonlinear pressure–strain models.

Applying the approximation of Rodi (1976) to remove the Reynolds-stress advection and diffusion terms,

$$\frac{\mathrm{D}}{\mathrm{D}t}(\overline{u_iu_j}) - \text{ diff }(\overline{u_iu_j}) \approx \frac{\overline{u_iu_j}}{k}\left(\frac{\mathrm{D}k}{\mathrm{D}t} - \text{ diff }(k)\right) = \frac{\overline{u_iu_j}}{k}(P-\varepsilon), \tag{10}$$

and assuming isotropic dissipation, the Reynolds-stress transport equations can be reduced to

$$(P-\varepsilon)a_{ij} = \left(P_{ij} - \frac{2}{3}P\delta_{ij}\right) + \Phi_{ij}, \tag{11}$$

where P_{ij} and Φ_{ij} are the production and pressure–strain correlations, respectively. The latter is typically decomposed into *slow* (Φ_{ij1}) and *rapid* (Φ_{ij2}) parts, which are most commonly based upon a linear model:

$$\begin{aligned}&\boldsymbol{\Phi}_1/\varepsilon = -C_1\mathbf{a},\\ &\boldsymbol{\Phi}_2/\varepsilon = C_{01}\mathbf{s} + C_{11}\left(\mathbf{as}+\mathbf{sa}-\frac{2}{3}\{\mathbf{as}\}\mathbf{I}\right) + C_{12}(\boldsymbol{\omega}\mathbf{a}-\mathbf{a}\boldsymbol{\omega}).\end{aligned} \tag{12}$$

For example, in the widely-used model of Launder et al. (1975), $C_1 = 1.8$, $C_{01} = 0.8$, $C_{11} = C_{12} = 0.6$. The algebraic system (11) can then be written as

$$\mathbf{a} = -\alpha\mathbf{s} - \beta\left(\mathbf{sa}+\mathbf{as}-\frac{2}{3}\{\mathbf{as}\}\mathbf{I}\right) - \gamma(\boldsymbol{\omega}\mathbf{a}-\mathbf{a}\boldsymbol{\omega}), \tag{13}$$

where

$$\alpha = \frac{4/3-C_{01}}{C_1+P/\varepsilon-1}, \qquad \beta = \frac{1-C_{11}}{C_1+P/\varepsilon-1}, \qquad \gamma = \frac{1-C_{12}}{C_1+P/\varepsilon-1} \tag{14}$$

and $\mathbf{a}$, $\mathbf{s}$, and $\boldsymbol{\omega}$ were defined in Section 2. The objective is to find an *explicit* representation for $\mathbf{a}$ in terms of $\mathbf{s}$ and $\boldsymbol{\omega}$.

Next, we introduce the iterative approach to the construction of the new NLEVM. Consider the general implicit system

$$\mathbf{a} = \mathbf{b} + \mathbf{f}(\mathbf{a}). \tag{15}$$

This may be approximated iteratively by the sequence

$$\mathbf{a}^{(1)} = \mathbf{b}; \qquad \mathbf{a}^{(n)} = \mathbf{b} + \mathbf{f}(\mathbf{a}^{(n-1)}), \qquad n = 2,3,4\ldots \tag{16}$$

This is only a formal iterative procedure, and no assumption is made about its convergence. If the same technique is applied to system (13), the following sequence is obtained.

$$\mathbf{a}^{(1)} = -\alpha\mathbf{s}. \tag{17}$$

This is obviously of a linear-EVM type. Iterating, according to Eq. (16),

$$\begin{aligned}\mathbf{a}^{(2)} &= -\alpha\mathbf{s} - \beta\left(\mathbf{sa}^{(1)}+\mathbf{a}^{(1)}\mathbf{s}-\frac{2}{3}\{\mathbf{a}^{(1)}\mathbf{s}\}\mathbf{I}\right) - \gamma\left(\boldsymbol{\omega}\mathbf{a}^{(1)}-\mathbf{a}^{(1)}\boldsymbol{\omega}\right)\\ &= -\alpha\mathbf{s} + 2\alpha\beta\left(\mathbf{s}^2 - \frac{1}{3}s_2\mathbf{I}\right) + \alpha\gamma(\boldsymbol{\omega}\mathbf{s}-\mathbf{s}\boldsymbol{\omega}).\end{aligned} \tag{18}$$

This is a quadratic NLEVM. Note that there is no $\boldsymbol{\omega}^2$ term. Iterating again leads to

$$\begin{aligned}\mathbf{a}^{(3)} &= -\alpha\mathbf{s} - \beta\left(\mathbf{s}\mathbf{a}^{(2)} + \mathbf{a}^{(2)}\mathbf{s} - \frac{2}{3}\{\mathbf{a}^{(2)}\mathbf{s}\}\mathbf{I}\right) - \gamma(\boldsymbol{\omega}\mathbf{a}^{(2)} - \mathbf{a}^{(2)}\boldsymbol{\omega}) \\ &= -\alpha\mathbf{s} + 2\alpha\beta\left(\mathbf{s}^2 - \frac{1}{3}s_2\mathbf{I}\right) + \alpha\gamma(\boldsymbol{\omega}\mathbf{s} - \mathbf{s}\boldsymbol{\omega}) \\ &\quad - 4\alpha\beta^2\left(\mathbf{s}^3 - \frac{1}{3}s_3\mathbf{I} - \frac{1}{3}s_2\mathbf{s}\right) - 3\alpha\beta\gamma(\boldsymbol{\omega}\mathbf{s}^2 - \mathbf{s}^2\boldsymbol{\omega}) \\ &\quad - \alpha\gamma^2(\boldsymbol{\omega}^2\mathbf{s} + \mathbf{s}\boldsymbol{\omega}^2 - 2\boldsymbol{\omega}\mathbf{s}\boldsymbol{\omega}). \end{aligned} \tag{19}$$

This is a cubic EVM. Iteration is concluded at this level. The last approximation can be written in more than one form, since the Cayley–Hamilton theorem applied to $\mathbf{s}$ and $\mathbf{s}+\boldsymbol{\omega}$ yields

$$\begin{aligned}&\mathbf{s}^3 - \frac{1}{3}s_3\mathbf{I} = \frac{1}{2}s_2\mathbf{s}, \\ &\boldsymbol{\omega}^2\mathbf{s} + \mathbf{s}\boldsymbol{\omega}^2 + \boldsymbol{\omega}\mathbf{s}\boldsymbol{\omega} - \{\boldsymbol{\omega}\mathbf{s}\boldsymbol{\omega}\}\mathbf{I} = \frac{1}{2}\omega_2\mathbf{s}.\end{aligned} \tag{20}$$

Substituting the resulting expressions for $\mathbf{s}^3$ and $\boldsymbol{\omega}\mathbf{s}\boldsymbol{\omega}$ in Eq. (19), one obtains a cubic stress–strain relationship in the canonical form (4):

$$\begin{aligned}\mathbf{a}^{(3)} &= -\alpha\mathbf{s} + 2\alpha\beta\left(\mathbf{s}^2 - \frac{1}{3}s_2\mathbf{I}\right) + \alpha\gamma(\boldsymbol{\omega}\mathbf{s} - \mathbf{s}\boldsymbol{\omega}) - \frac{2}{3}\alpha\beta^2 s_2\mathbf{s} \\ &\quad - 2\alpha\gamma^2\omega_2\mathbf{s} - 3\alpha\gamma^2\left(\boldsymbol{\omega}^2\mathbf{s} + \mathbf{s}\boldsymbol{\omega}^2 - \omega_2\mathbf{s} - \frac{2}{3}\{\boldsymbol{\omega}\mathbf{s}\boldsymbol{\omega}\}\mathbf{I}\right) \\ &\quad - 3\alpha\beta\gamma(\boldsymbol{\omega}\mathbf{s}^2 - \mathbf{s}^2\boldsymbol{\omega}). \end{aligned} \tag{21}$$

In principle, the parent DSM gives the values of α, β, γ according to Eq. (14). However, these will not be appropriate for wall-bounded flows, because the expression for Φ_{ij} included no wall-reflection or viscous effects, and the algebraic-stress simplifications – in particular, the assumption of isotropic dissipation – become untenable in the viscous sublayer. In the present model, the role of the DSM is to provide the *relationship between coefficients*, with free parameters α, β, and γ calibrated to return the correct behaviour of all stresses in a simple shear flow.

3.3. Calibration in simple shear

In simple shear, where $\partial U/\partial y$ is the only nonzero velocity derivative, the cubic model (21) gives, for the three independent anisotropy components,

$$\begin{aligned}a_{11} &= \overline{u^2}/k - 2/3 = \frac{1}{6}(\alpha\beta + 3\alpha\gamma)\sigma^2, \\ a_{22} &= \overline{v^2}/k - 2/3 = \frac{1}{6}(\alpha\beta - 3\alpha\gamma)\sigma^2, \\ a_{12} &= \overline{uv}/k = -\frac{1}{2}\alpha\sigma\left[1 - \left(\gamma^2 - \frac{1}{3}\beta^2\right)\sigma^2\right], \end{aligned} \tag{22}$$

where the tensorially-invariant shear parameter $\sigma = (k/\varepsilon)\sqrt{(\partial U_i/\partial x_j)^2}$ here reduces to $\sigma = (k/\varepsilon)\partial U/\partial y$. The essence of the calibration is simple: by determining a_{ij} and σ as functions of y^* from some fundamental flow, indicated henceforth by a tilde, Eq. (22) can be inverted for α, β, and γ. This leads to

$$\begin{aligned}&\alpha\tilde{\sigma} = -\tilde{a}_{12} + \sqrt{\tilde{a}_{12}^2 + (\tilde{a}_{11} - \tilde{a}_{22})^2 - 3(\tilde{a}_{11} + \tilde{a}_{22})^2}, \\ &\beta\tilde{\sigma} = \frac{3(\tilde{a}_{11} + \tilde{a}_{22})}{\alpha\tilde{\sigma}}, \qquad \gamma\tilde{\sigma} = \frac{\tilde{a}_{11} - \tilde{a}_{22}}{\alpha\tilde{\sigma}}. \end{aligned} \tag{23}$$

The process bears some resemblance to the *calibration* (although not the *derivation*) of the quadratic model of Speziale (1987).

In establishing $\tilde{a}_{ij}$, two limiting values are known: $\tilde{a}_{22}(0) = -2/3$ and $\tilde{a}_{12}(0) = 0$, since $\overline{v^2}/k \to 0$ as $y^* \to 0$. For general functional forms, it is possible to use DNS data for some fundamental shear flow: for example, a zero-pressure-gradient boundary layer (Spalart, 1988) or fully-developed channel flow (Kim et al., 1987, and related unpublished data). In each case, stress components are given as functions of $y^+ = y_n u_\tau/\nu$, where $u_\tau = (\tau_w/\rho)^{1/2}$ and τ_w is the wall shear stress. As y^+ will generally be unavailable in a complex flow, these are re-plotted as functions of y^*, although it is acknowledged that y^* will not necessarily be monotonic with distance from the wall. A distance-free formulation could be obtained through use of R_t rather than y^*, but the experience of the present authors is that y^* is a far more representative wall-distance indicator and tends to be more numerically stable. The variations of the normalised Reynolds stresses and the dimensionless shear parameter are plotted in Fig. 2, for boundary-layer and channel flow at various Reynolds numbers, together with the following curve fits, having the correct asymptotic behaviour for small y^* and in the log-law region, to the channel-flow data at the larger Reynolds number:

$$\begin{aligned}&\overline{u^2}/k = 1 + 0.42\exp(0.296y^{*1/2} - 0.040y^*), \\ &\overline{v^2}/k = 0.404[1 - \exp(-0.001y^* - 0.000147y^{*2})], \\ &-\overline{uv}/k = 0.3[1 - \exp(-0.00443y^{*1/2} - 0.0189y^*)], \end{aligned} \tag{24}$$

and

$$\tilde{\sigma} = 3.33[1 - \exp(-0.45y^*)][1 + 0.277y^{*3/2}\exp(-0.088y^*)]. \tag{25}$$

Considering first the high-Re regime, i.e., letting $y^* \to \infty$ in Eq. (24), and denoting variables in this limit by a subscript ∞, one obtains

$$\begin{aligned}&\overline{\alpha} \equiv \alpha_\infty\tilde{\sigma}_\infty = 0.96, \qquad \overline{\beta} \equiv \beta_\infty\tilde{\sigma}_\infty = 0.22, \\ &\overline{\gamma} \equiv \gamma_\infty\tilde{\sigma}_\infty = 0.62. \end{aligned} \tag{26}$$

A feature of the present model is that both linear and cubic terms contribute to the shear stress in simple shear, since the terms in $s_2\mathbf{s}$ and $\omega_2\mathbf{s}$ do not cancel. If α, β, and γ are evaluated according to Eq. (23) for all y^*, it is found that both the linear term $(-\alpha\mathbf{s})$ and the cubic terms are O(1) as $y^* \to 0$, and only in combination do they yield an expression for a_{12}, which vanishes as $y^* \to 0$. To ensure that each individually vanishes as $y^* \to 0$, we replace β and γ *in the cubic terms* by β' and γ', so that

$$\beta'\tilde{\sigma} = \beta_\infty\tilde{\sigma}_\infty = \overline{\beta}, \qquad \gamma'\tilde{\sigma} = \gamma_\infty\tilde{\sigma}_\infty = \overline{\gamma}. \tag{27}$$

From Eq. (22), the expression for α in Eq. (23) must then be amended in the viscous sublayer:

$$\alpha = 2\frac{(-\tilde{a}_{12})}{\tilde{\sigma}}\left(1 + \frac{1}{3}\overline{\beta}^2 - \overline{\gamma}^2\right)^{-1}. \tag{28}$$

The expression for the quadratic coefficients remains unchanged. This minor variation can be justified on the grounds that the algebraic Reynolds-stress model is strictly invalid in the viscous sublayer and that the requirement is to make a smooth transition to a model consistent with observed near-wall anisotropy components.

3.4. Extension to nonequilibrium conditions

The calibration above assumes equilibrium conditions and it is pertinent to consider how departures from equilibrium may be modelled. From the actual flow field, it is possible to calculate *local* strain parameters $\overline{s} = (2s_{ij}s_{ij})^{1/2}$, $\overline{\omega} = (2\omega_{ij}\omega_{ij})^{1/2}$ and $\sigma = (s_{ij}s_{ij} + \omega_{ij}\omega_{ij})^{1/2} = (k/\varepsilon)\sqrt{(\partial U_i/\partial x_j)^2}$,

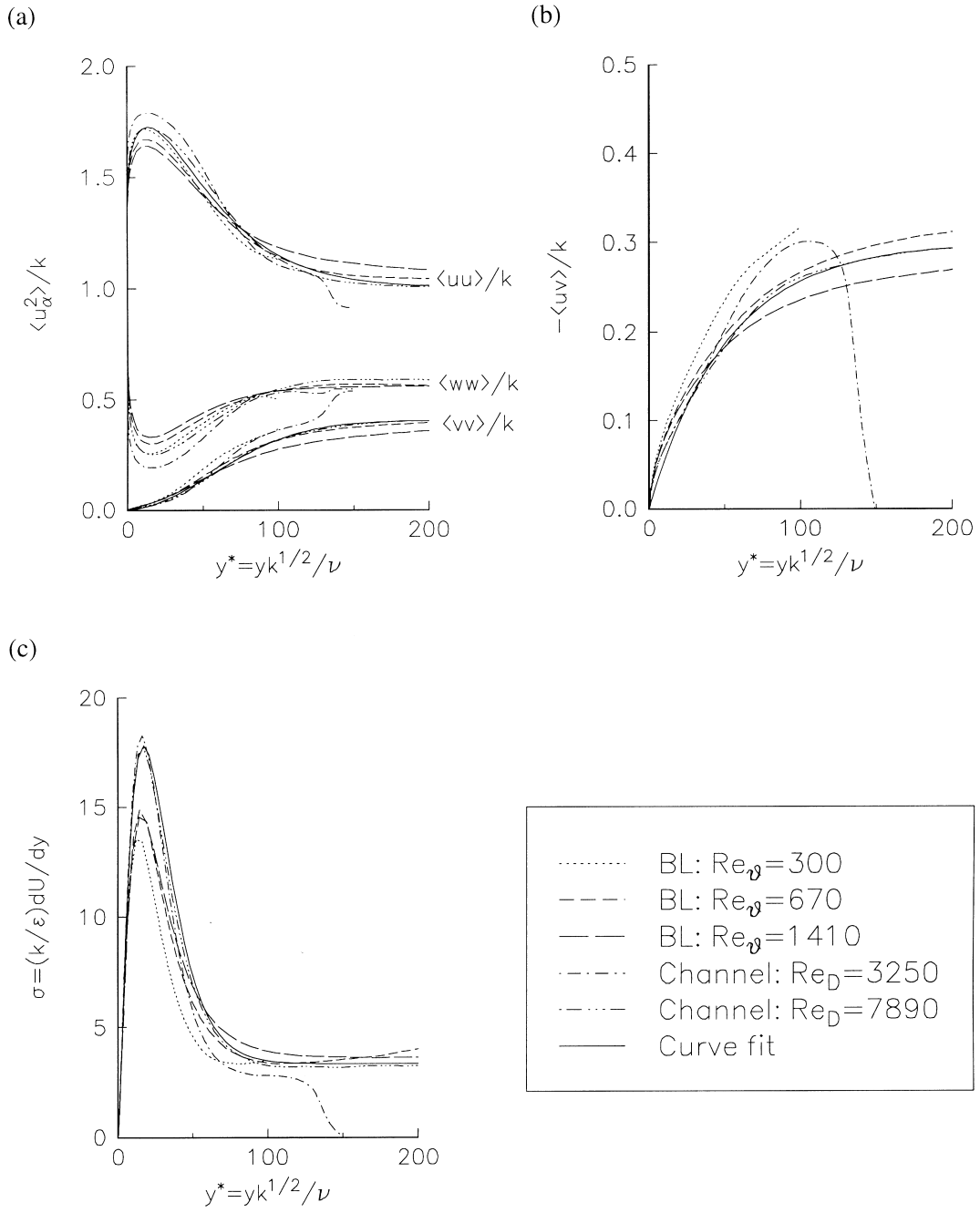

Fig. 2. Profiles of normalised stresses and shear parameter from DNS data: (a) normal stresses; (b) shear stress; (c) shear parameter.

which all reduce to $\tilde{\sigma}$ in the calibration flow. Thus, it is permissible to multiply α, β, and γ by functions of the form $f_P(\overline{s}/\tilde{\sigma}, \overline{\omega}/\tilde{\sigma})$ or $f_P(\sigma/\tilde{\sigma})$, which are unity when $\overline{s} = \overline{\omega} = \tilde{\sigma}$. Now, although the values of α, β, and γ from the original DSM (Eq. (14)) are not used, it is observed that each has the *same* P/ε-dependence through the factor $(C_1 + P/\varepsilon - 1)^{-1}$. This indicates the typical variation of coefficients as the flow departs from the simple shear flow in which they were calibrated – in particular the behaviour for large strains – and suggests a multiplicative factor,

$$f_P = \frac{C_1 + \tilde{P}/\varepsilon - 1}{C_1 + P/\varepsilon - 1}, \tag{29}$$

in each of α, β, and γ, where the tilde signifies, as usual, conditions in the calibration flow. The direct use of Eq. (29) is found to lead to numerical instability. Instead, P/ε is *approximated* by $f_P \tilde{C}_\mu \sigma^2$. We discuss this approximation, and the value of $\tilde{C}_\mu$, below. Inverting Eq. (29) for f_P yields

$$f_P = \frac{2f_0}{1 + \sqrt{1 + 4f_0(f_0 - 1)(\sigma/\tilde{\sigma})^2}}, \tag{30}$$

where $f_0 = 1 + \tilde{C}_\mu \tilde{\sigma}^2/(C_1 - 1)$.

In fact, relation (30) ensures that $f_P = 1$ when $\sigma = \tilde{\sigma}$, regardless of f_0. The anisotropy components will be assured bounded if $f_P \leqslant K(\tilde{\sigma}/\sigma)$, where K is a constant *independent of* y^*, and for this we require $(f_0 - 1)$ strictly greater than zero.

This is accomplished by taking $\tilde{C}_\mu\tilde{\sigma}^2 = \max(0.09\tilde{\sigma}^2, 1.0)$, which is formally true only in the log-law region. With $C_1 = 1.8$ in accordance with the DSM, f_0, the value of f_P in the absence of mean strain, is given by

$$f_0 = 1 + 1.25\max(0.09\tilde{\sigma}^2, 1.0). \tag{31}$$

The boundedness requirement in flows with large rotational strains is also the reason for assuming $P/\varepsilon \propto \sigma^2$ rather than $P/\varepsilon \propto \bar{s}^2$, as would be the case for linear models. Note that *boundedness* is a weaker condition than *realisability* – all normal stresses positive and the Schwarz inequality satisfied – which is much harder to impose in a low-Re model, since $\overline{v}^2/k$ tends to its theoretical lower bound of zero as the wall is approached.

To summarise, the final cubic, low-Re stress–strain relationship has the canonical form (4) with

$$\begin{aligned}
&C = \frac{\left(-\tilde{a}_{12}\right)}{\tilde{\sigma}}\left(1 + \frac{1}{3}\overline{\beta}^2 - \overline{\gamma}^2\right)^{-1} f_P,\\
&q_1 = \frac{6(\tilde{a}_{11} + \tilde{a}_{22})}{\tilde{\sigma}^2} f_P^2, \qquad q_2 = \frac{\tilde{a}_{11} - \tilde{a}_{22}}{\tilde{\sigma}^2} f_P^2, \qquad q_3 = 0,\\
&\gamma_1 = \frac{4}{3}C(\overline{\beta}/\tilde{\sigma})^2 f_P^2, \qquad \gamma_2 = 4C(\overline{\gamma}/\tilde{\sigma})^2 f_P^2, \qquad \gamma_3 = 6C(\overline{\gamma}/\tilde{\sigma})^2 f_P^2,\\
&\gamma_4 = 6C(\overline{\beta}/\tilde{\sigma})(\overline{\gamma}/\tilde{\sigma}) f_P^2,
\end{aligned} \tag{32}$$

where $\overline{\beta}$ and $\overline{\gamma}$ are given by Eq. (26) and f_P by Eqs. (30) and (31). Simple-shear-flow values of anisotropy components $\tilde{a}_{ij}$ and shear parameter $\tilde{\sigma}$ are derived from Eqs. (24) and (25), respectively.

When the first two cubic terms are compounded with the linear term, the stress–strain relationship may be written as

$$\begin{aligned}
\mathbf{a} = {} & \frac{\tilde{a}_{12}}{\tilde{\sigma}}\left[\frac{1 + \left\{\frac{1}{3}\overline{\beta}^2(\overline{s}/\tilde{\sigma})^2 - \overline{\gamma}^2(\overline{\omega}/\tilde{\sigma})^2\right\} f_P^2}{1 + \frac{1}{3}\overline{\beta}^2 - \overline{\gamma}^2}\right] f_P(2\mathbf{s})\\
& + q_1\left(\mathbf{s}^2 - \frac{1}{3}s_2\mathbf{I}\right) + q_2(\boldsymbol{\omega}\mathbf{s} - \mathbf{s}\boldsymbol{\omega}) + (\text{additional cubic terms}),
\end{aligned} \tag{33}$$

where, in any 2-D incompressible flow, the third line vanishes, and only the first line contributes to the production of turbulent kinetic energy. The term bracketed [.] represents a curvature-dependent factor. However, because it is not unconditionally positive, it cannot be assimilated into a curvature-dependent C_μ.

3.5. Turbulence transport equations

We adopt here the construction of Lien and Leschziner (1993) in writing the modelled low-Re k and ε transport equations as

$$\frac{\mathrm{D}k}{\mathrm{D}t} = \nabla.[(\nu + \nu_t/\sigma_k)\nabla k] + P - \varepsilon \tag{34}$$

and

$$\frac{\mathrm{D}\varepsilon}{\mathrm{D}t} = \nabla.[(\nu + \nu_t/\sigma_\varepsilon)\nabla\varepsilon] + [C_{\varepsilon 1}P - C_{\varepsilon 2}(\varepsilon - D\varepsilon_w)]\frac{\varepsilon}{k}, \tag{35}$$

where

$$\varepsilon_w = \frac{k^{3/2}}{\tilde{l}_\varepsilon}. \tag{36}$$

$\tilde{l}_\varepsilon$ is an algebraic approximation for the near-wall dissipation length scale (see below) and D is a damping function that vanishes in the high-R_t regime. The constants are $C_{\varepsilon 1} = 1.44$, $C_{\varepsilon 2} = 1.83$ and $\sigma_k = 1.0$. $\sigma_\varepsilon = \kappa^2/C_{\mu\infty}^{1/2}(C_{\varepsilon 2} - C_{\varepsilon 1}) = 1.37$, to be consistent with the log-law of the wall. The above value for $C_{\varepsilon 2}$ is increasingly being used in preference to the more familiar 1.92, and is found to be markedly better in flows with large streamwise pressure gradients. Note that both k and ε equations assume isotropic diffusion based on an eddy-viscosity $\nu_t = C_\mu k^2/\varepsilon$, where

$$C_\mu = \frac{\left(-\tilde{a}_{12}\right)}{\tilde{\sigma}} f_P. \tag{37}$$

In this case C_μ is not equal to C in the first line of the stress–strain constitutive relation, because cubic terms (proportional to **s**) also contribute to the balance in simple shear. A numerically equivalent (but more convenient) treatment, however, is to set $C_\mu = C$ and apply compensating factors $(1 + \frac{1}{3}\overline{\beta}^2 - \overline{\gamma}^2)^{-1}$ to σ_k and σ_ε.

The additional low-Re source term in the ε equation is designed to return a length scale close to an algebraic form $\tilde{l}_\varepsilon$ as the wall is approached. This form is based on an approximation to the DNS data used earlier to calibrate the stress–strain coefficients:

$$\tilde{l}_\varepsilon = ay(1 + b/y^*)[1 - \exp(-y^{*2}/2ab)], \tag{38}$$

where $a = 1.09$, $b = 128$. Apart from providing a satisfactory curve fit (Fig. 3), this is so constructed as to conform to the theoretical asymptotic behaviour ($\varepsilon \sim 2\nu k/y^2$, $l_\varepsilon \sim yy^*/2$) as $y^* \to 0$ and to a linear variation, albeit with an offset, in the log-law region. It should be remarked, however, that, unlike the normalised stress components (Fig. 2), DNS predictions of l_ε vary significantly with geometry and Reynolds number.

When the new nonlinear stress–strain relationship is used to calculate channel flow, it is found that the *normalised* stresses $\overline{u_i u_j}/k$ are relatively insensitive to the modelling of the ε equation. The *absolute* values of the stresses are, however, dependent on a good representation of k and hence on the low-Re terms in the dissipation-rate equation. A careful calibration in channel flow yields the damping function

$$D = \mathrm{e}^{-0.0038y^{*2}}. \tag{39}$$

The resulting mean-velocity and stress profiles are compared with DNS data in Fig. 4.

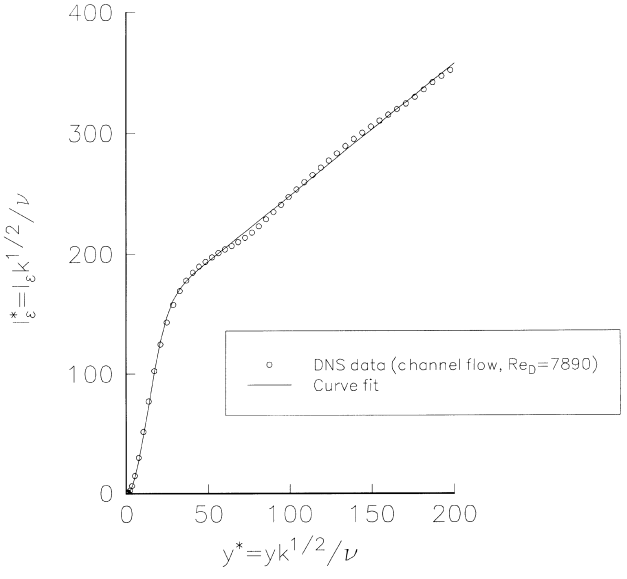

Fig. 3. Channel flow at $Re_D = 7890$ – dissipation length.

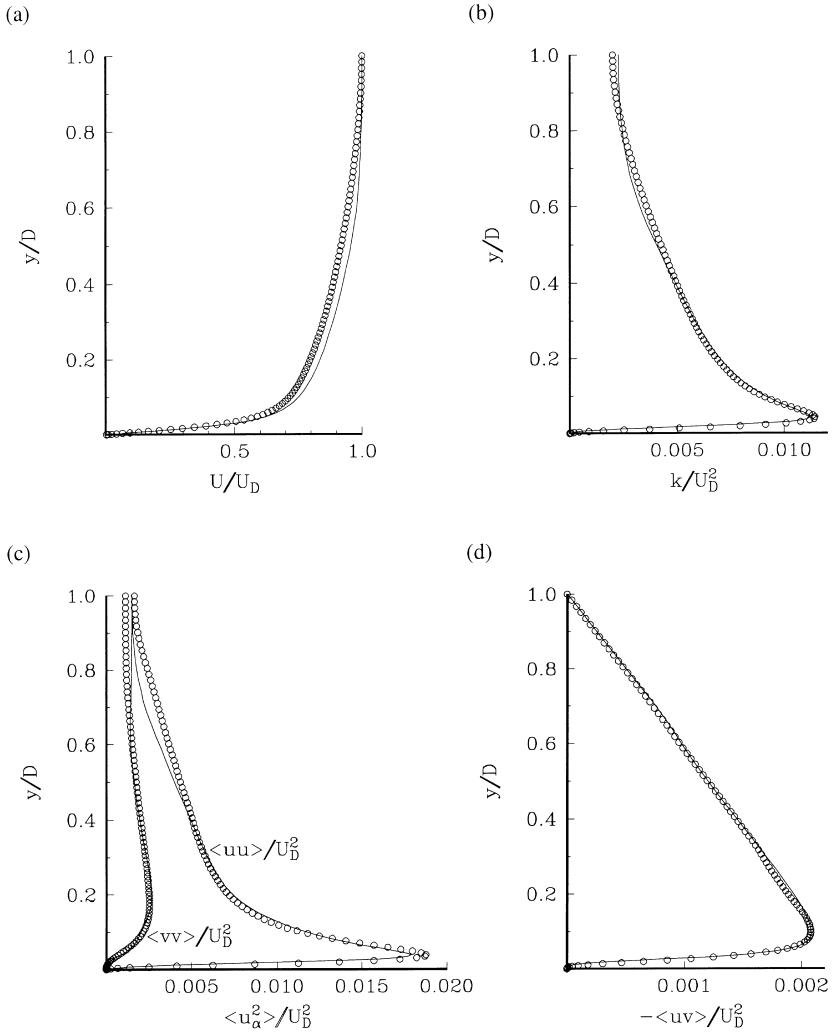

Fig. 4. Channel flow at $Re_D = 7890$: (a) mean velocity; (b) turbulent kinetic energy; (c) normal stresses; (d) shear stress.

4. Comparison with experiment

4.1. Numerical procedures and models tested

The performance of the present nonlinear $k-\varepsilon$ model has been examined against other two-equation models for a number of 2-D test cases (Fig. 5). Calculations were performed with a modified version of the finite-volume code STREAM (Lien and Leschziner, 1994), using nonstaggered variable storage on single-block, structured, nonorthogonal grids. The steady-state, incompressible flow equations for primitive variables were solved iteratively, using the SIMPLE pressure-correction algorithm and line-iterative procedures to solve the discretised equations. The advective fluxes of all variables were approximated by the second-order, upwind-biased, bounded UMIST scheme (Lien and Leschziner, 1994) – a total-variation-diminishing implementation of the QUICK scheme – and the mass fluxes on cell faces obtained by the Rhie–Chow interpolation procedure.

Besides predictions with the new cubic model, results for a number of other low-Re two-equation models have been included. These are: the linear $k-\varepsilon$ model of Lien and Leschziner (1993); a quadratic version formed by including the nonlinear terms of Speziale (1987); and the cubic model of Lien et al. (1996). Besides the inclusion of cubic terms, the new model and that of Lien et al. differ from the other two in using coefficients that are sensitised to strain and vorticity

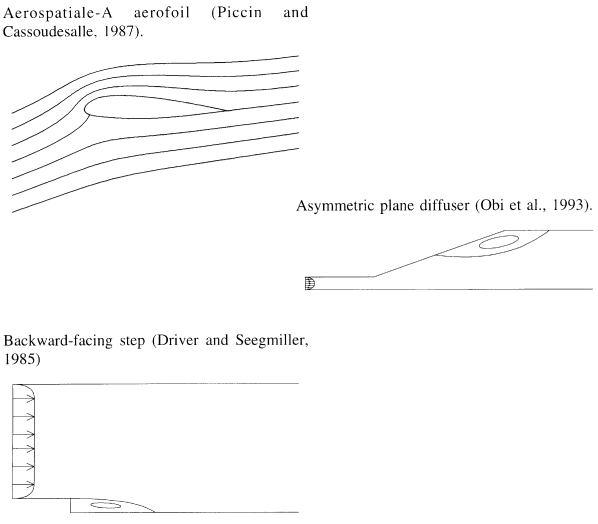

Fig. 5. 2-D test cases.

invariants, a feature found necessary to suppress the excessive generation of turbulence in flows with large streamwise strains.

4.2. High-lift aerofoil (Piccin and Cassoudesalle, 1987)

The Aerospatiale-A aerofoil is an example of a single-element profile operating at or near stall, and hence the fluid-dynamical problem is one of predicting separation in an adverse pressure gradient from the curved suction surface. Detailed LDA measurements of mean velocity and turbulent stresses were made for the angles of attack 7.2° and 13.3° (corrected for blockage effects) at $\mathrm{Re} = 2.1 \times 10^6$ (based on chord c and free-stream velocity U_0) and $\mathrm{Ma} = 0.15$. For the present purpose, this flow can be regarded as incompressible. Transition occurred at 12 and 30% of chord on suction and pressure surfaces, respectively, and these locations were specified in the calculations. Flow separation was observed at the larger incidence angle, on which computations have focused.

This test case was part of the EUROVAL code-validation exercise (Haase et al., 1993) and the mandatory C-type grid used in that comparison was adopted here. This contains 352 $\times$ 64 control volumes and extends to $10c$ from the aerofoil surface. The position of the near-wall grid node corresponds to a maximum y^+ value of about 0.5. Uniform boundary conditions, with $k/U_0^2 = 10^{-4}$ and $l_\varepsilon/c = 1/60$, were applied at the inflow boundary and zero-gradient conditions assumed at the outflow boundary. The imposition of a circulation, based on the experimentally-determined lift, at the outer boundary was found to have an insignificant effect on the predicted flow close to the aerofoil.

Computed mean velocity and turbulent-stress profiles are compared with experimental measurements near the separation point on the suction surface in Fig. 6. The retarding effect of the adverse pressure gradient is best predicted by the new model, although none of the models tested show separation. With the linear k–ε model the normal stresses are almost equal in magnitude, whereas the inclusion of quadratic terms results in a qualitatively correct, though slightly exaggerated, degree of anisotropy. The normal-stress profiles are most accurately represented by the new model and that of Speziale (1987), which were both calibrated against wall-parallel flows. Curvature effects are, apparently, quite weak.

Pressure and skin-friction coefficients are plotted in Fig. 7. These coefficients are of great importance in establishing aero-

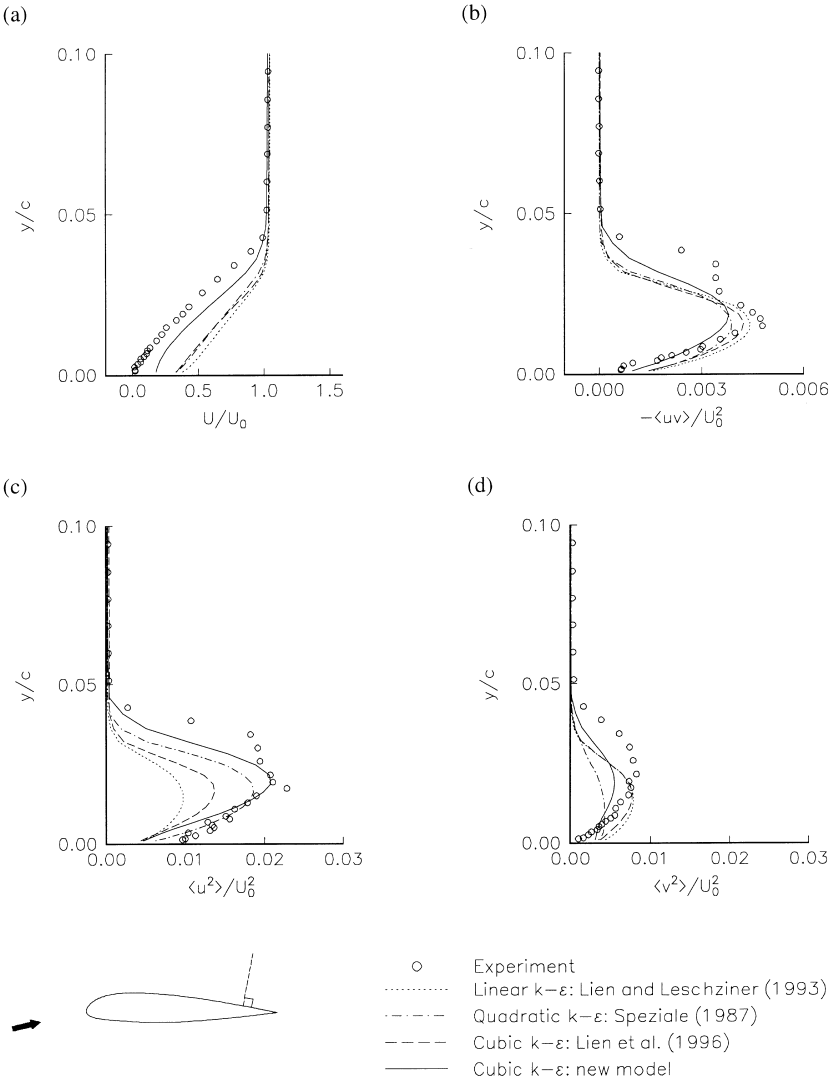

Fig. 6. Aerofoil – mean velocity and turbulence profiles at 82.5% chord: (a) mean velocity; (b) shear stress; (c) streamwise velocity variance; (d) wall-normal velocity variance.

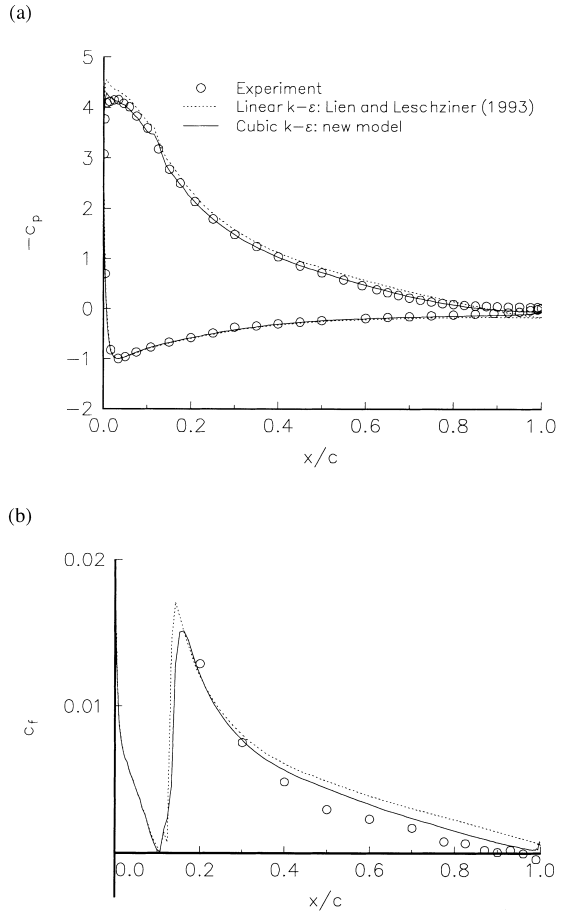

Fig. 7. Aerofoil – surface coefficients: (a) pressure coefficient; (b) skin friction.

foil characteristics. In addition to generally better prediction of the pressure and surface drag over the suction surface, the new model is seen to suppress the anomalous peak in negative pressure near the leading edge. Since this lies within the laminar region, it cannot be connected to the local turbulence closure and reflects the sensitive coupling between the trailing-edge and leading-edge flow via circulation-related constraints.

4.3. Plane asymmetric diffuser (Obi et al., 1993)

This case involves separation from a plane wall and reattachment in the duct following the diffusing section. The diffusing section has a length of $21H$, where H is the inlet channel height, and overall expansion ratio of 4.7. The corners are rounded with arcs of radius $4.3H$. The Reynolds number based on upstream centre-line velocity and H is 21,200. Fully-developed profiles of U and $\overline{u^2}$ were provided at a distance $11H$ upstream of the diffuser section. Mean-velocity and turbulence profiles were measured by LDA at various stations, together with pressure distributions on the walls. The flow was observed to separate from the angled wall because of the adverse pressure gradient at $x/H \approx 11$, measured from the start of the diffuser, and to reattach at $x/H \approx 26$.

The finite-volume mesh contained 270×80 control volumes and extended from $x/H = -11$ to $x/H = 60$. Inlet velocity and turbulence energy were specified using the experimental data and the approximation $k = \overline{u^2}$ for fully-developed channel flow. ε was determined from a simple algebraic model for the dissipation length.

The development of the mean-velocity profile along the diffuser is shown in Fig. 8. Although all nonlinear models provide an improvement on the linear k–ε model in resolving the strong cross-channel asymmetry observed in the experiment, the best agreement is obtained with those models whose coefficients are sensitised to the strain invariants, which helps to counter the generation of excessive near-wall turbulent length scales in strong streamwise pressure gradients. By far the best

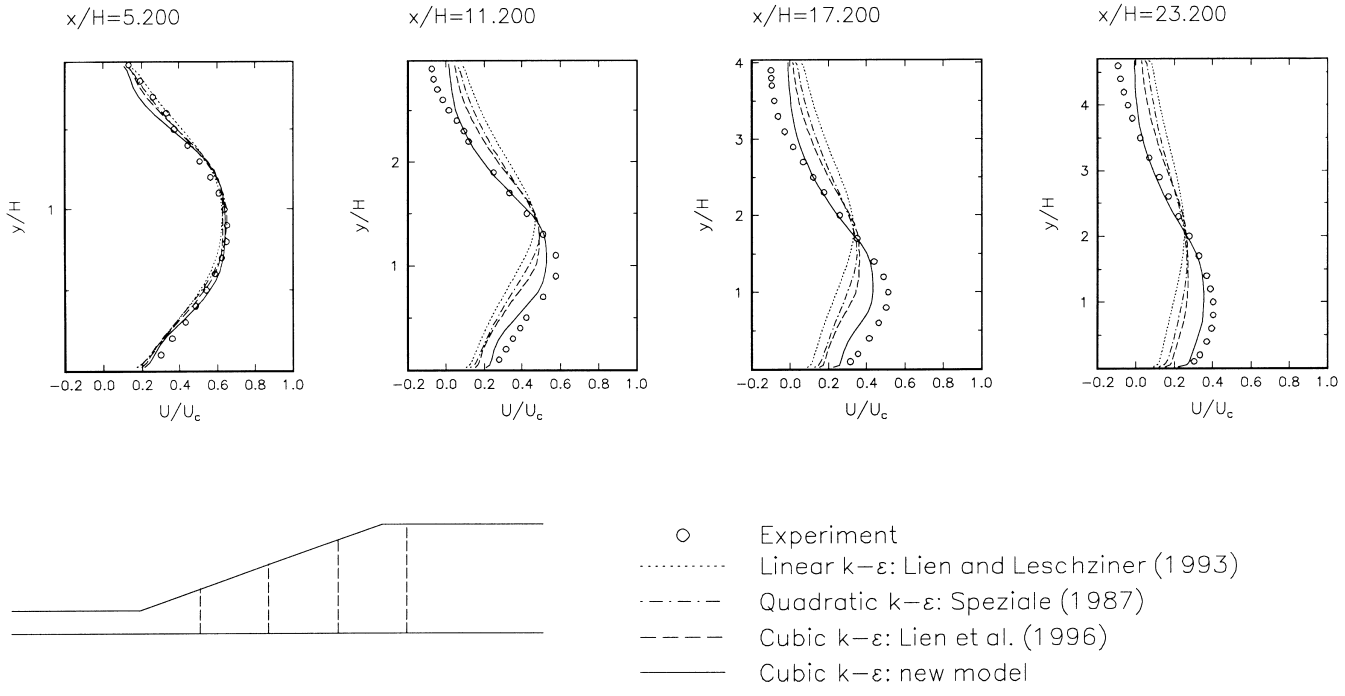

Fig. 8. Diffuser – development of mean-velocity profile.

agreement is obtained with the new cubic model, which is also the only model to predict separation from the sloping wall. Fig. 9 shows mean-velocity and turbulent-stress profiles near the centre of the diffuser and confirms that nonlinear models can correctly predict the asymmetric stress profiles and the level of anisotropy. Again, the new cubic model produces good agreement with the experimentally-derived data, the tendency, as with the aerofoil, being to exaggerate anisotropy slightly.

4.4. Backward-facing step (Driver and Seegmiller, 1985)

Driver and Seegmiller (1985) conducted a series of LDA measurements for backstep flows at a number of upper-wall inclination angles. The present calculations were for the simplest case of zero inclination, representing a sudden, one-sided, 1:9/8 expansion. Flow conditions upstream of the step were well-developed, with Reynolds number (based on mid-stream reference velocity U_r and step height H) of 38,000 and boundary-layer height $1.5H$.

Calculations were performed on a rectilinear mesh of 152×112 control volumes, with cells "blocked out" within the step to maintain a single-block, structured grid. Variable mesh spacing was used, with minimum control-volume height $0.0016H$ at all walls. This was to give $y^+ = 1$ at the near-wall node at inflow ($x/H = 4$, with x measured from the step). Additional refinement was made near the experimental reattach-

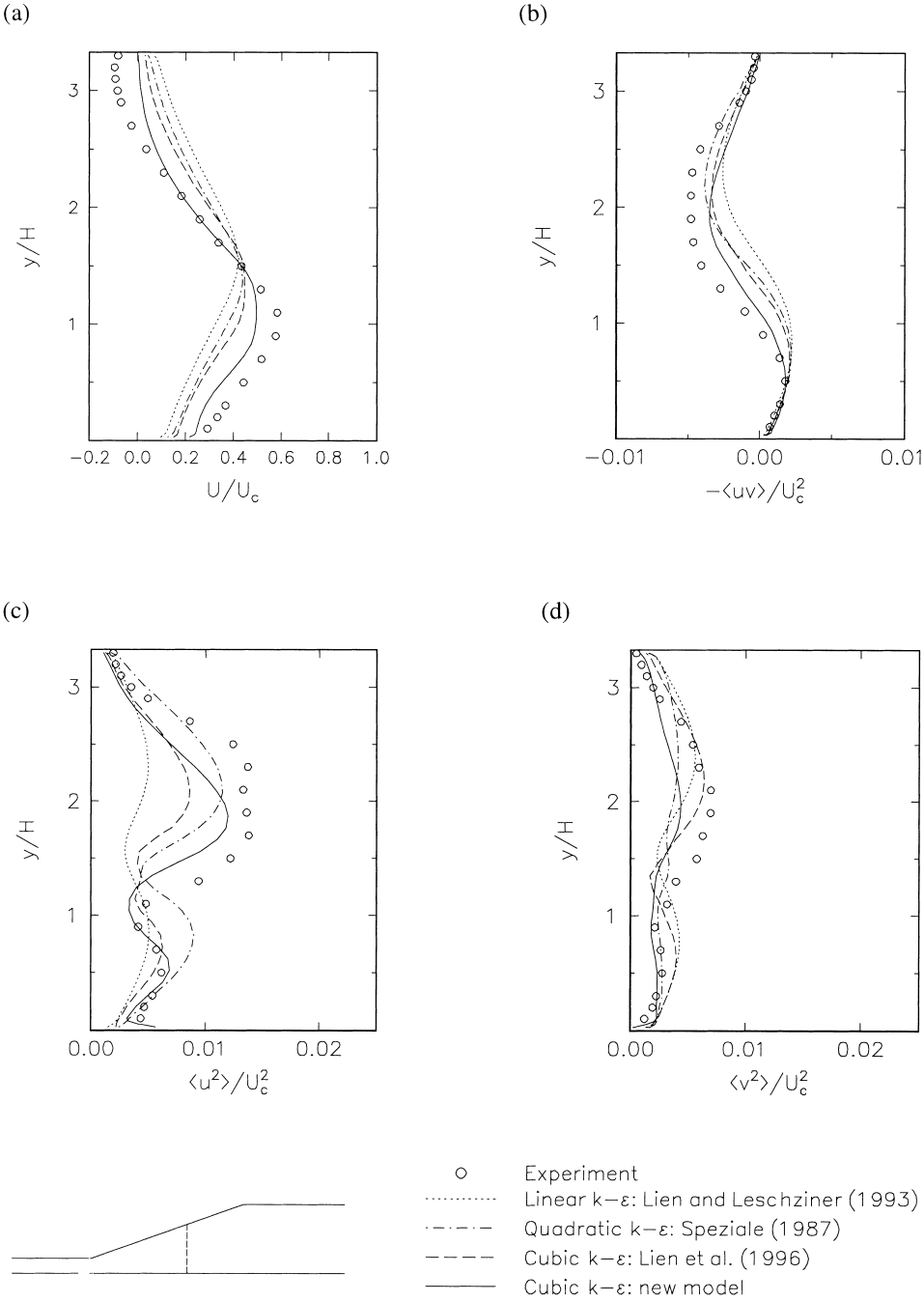

Fig. 9. Diffuser – mean-velocity and turbulence profiles at $x/H = 13$: (a) mean velocity; (b) shear stress; (c) streamwise velocity variance; (d) cross-stream velocity variance.

ment point, $x = 6.26H$, as determined from oil-film measurements. Flow variables were fixed by the experimental data at inflow.

Fig. 10 shows profiles of mean velocity and Reynolds stresses in the recirculating-flow region. In contrast to the constant-C_μ linear and quadratic models, the strain-sensitive models of Lien et al. (1996) and that described in the present paper, both underpredict the turbulence levels in the separated shear layer. This leads to overprediction of re-attachment length, a reduced backflow velocity, and a deeper recirculating-flow region. A similar behaviour has been observed in computations of separation behind a 2-D hill (Almeida et al., 1993). Above the separation streamline, the model behaviour is in accordance with that deduced for simple shear: the addition of quadratic terms tends to increase $\overline{u^2}$ and diminish $\overline{v^2}$, but has very little effect on the shear stress.

Fig. 11 shows surface-pressure and skin-friction coefficients downstream of the step. The former is particularly sensitive to the *shape* of the separation bubble, and the curves here are consistent with the deeper recirculating-flow region predicted by all the nonlinear models, though most significantly by the closures with strain-sensitive coefficients. All models overestimate the rate of recovery in the wake, where there is a discrepancy between the re-attachment position determined

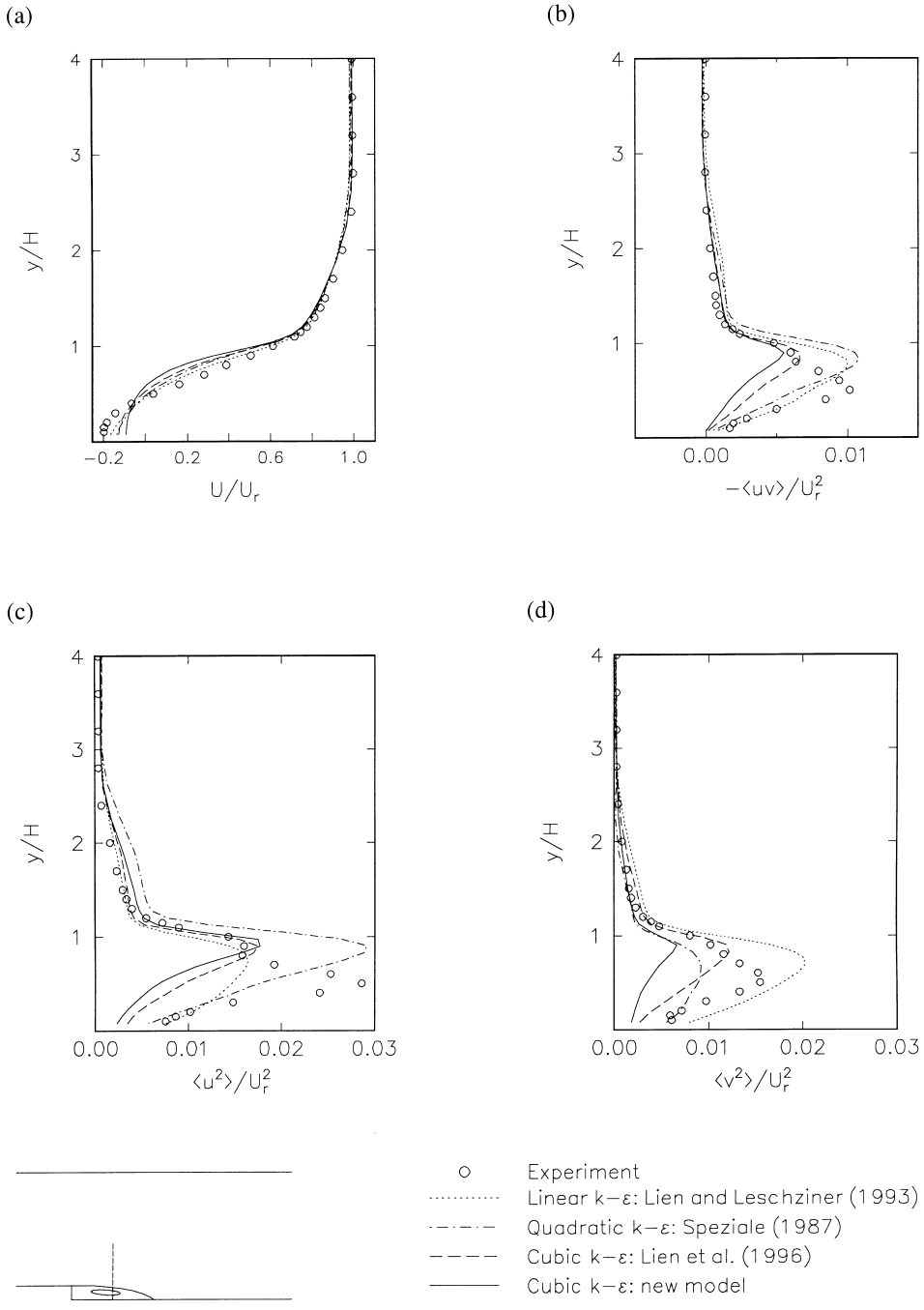

Fig. 10. Backward-facing step – mean-velocity and turbulence profiles at $x/H = 3$: (a) mean velocity; (b) shear stress; (c) streamwise velocity variance; (d) cross-stream velocity variance.

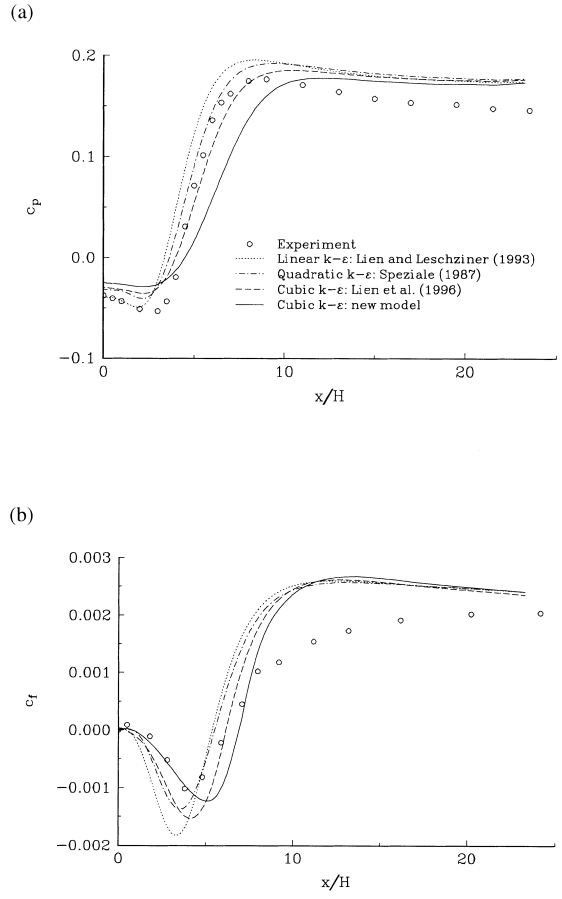

Fig. 11. Backward-facing step – surface coefficients: (a) pressure coefficient; (b) skin friction.

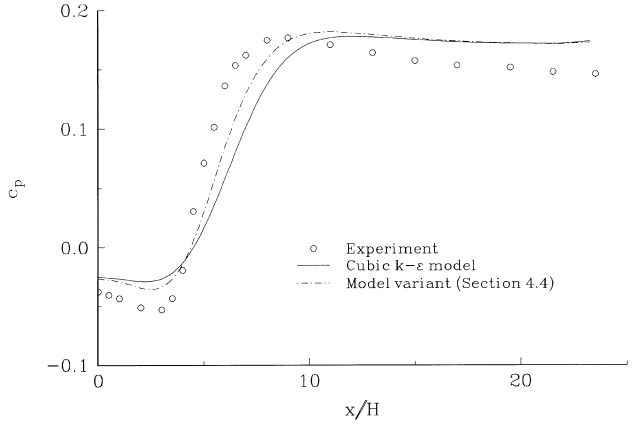

Fig. 12. Backward-facing step – surface pressure coefficient with the new cubic model and with the empirical modification of Section 4.4.

experimentally from oil-film techniques and that suggested by the mean-velocity profile.

The apparently poor performance of the new model in this test case can be traced to the nonequilibrium dependence represented by the factor f_P. In both this model and that of Lien et al. (1996) the appearance of the strain rate in the denominator of the effective C_μ has the effect of damping turbulent transport too much in the separated shear layer. On the other hand, such a strain-dependent linear coefficient is beneficial in suppressing excessive turbulence generation in flows with large streamwise pressure gradients, besides being necessary to maintain the theoretical constraint of bounded anisotropy components. A slightly-modified version of the new cubic model, based on Eq. (33), but with $(f_P/\tilde{\sigma})^2$ replaced by $(1/\sigma)^2$ in the curvature-dependent C_μ, was found to improve the pressure (Fig. 12) and skin-friction coefficients somewhat. However, this empirical adjustment had a detrimental effect in the other test cases reported here and has not been pursued further.

5. Conclusions

The capacity of models based upon a nonlinear stress–strain relationship to compute complex flows has been assessed, both theoretically and for a number of 2-D test cases. A new cubic model has been proposed, in which the relationship between coefficients is determined by the iterative solution of algebraic equations approximating the differential Reynolds-stress equations, with free parameters calibrated by reference to DNS data for channel flow. Coefficients are further sensitised to the local shear invariant in a manner that ensures that anisotropy components are bounded.

Besides an accurate representation of all stresses in channel flow, which was used for model calibration, the new nonlinear eddy-viscosity model has been demonstrated to offer superior performance to several other linear and nonlinear schemes in aerofoil and diffuser flows, where separation is not guaranteed by the geometry. The model performs less satisfactorily in massively-separated flows, where it exhibits a tendency to overpredict the length to re-attachment, because of insufficient turbulence energy generated in the curved shear layer. This behaviour is associated with the sensitivity of the coefficients to the strain and vorticity invariants and is similar to that displayed by other models of the bounded or realisable type.

Acknowledgements

The authors gratefully acknowledge the financial support of BMW, Mercedes-Benz, Opel, Audi, Renault, and Porsche, which made possible the preparation of this paper.

References

Almeida, G.P., Durao, D.F.G., Heitor, M.V., 1993. Wake flows behind two-dimensional model hills. Exp. Thermal Fluid Sci. 7, 87–101.

Craft, T.J., Launder, B.E., Suga, K., 1997. Prediction of turbulent transitional phenomena with a nonlinear eddy-viscosity mode. Int. J. Heat Fluid Flow 18, 15–28.

Driver, D.M., Seegmiller, H.L., 1985. Features of a reattaching turbulent shear layer in divergent channel flow. AIAA J. 163, 163–171.

Gatski, T.B., Speziable, C.G., 1993. On explicit algebraic stress models for complex turbulent flows. J. Fluid Mech. 254, 59–78.

Haase, W., Brandsma, F., Elsholz, E., Leschziner, M., Schwamborn, D., 1993. EUROVAL – A European initiative on validation of CFD codes. Notes Numer. Fluid Mech. 42, Vieweg.

Kim, J., Moin, P., Moser, R., 1987. Turbulence statistics in fully-developed channel flow at low Reynolds number. J. Fluid Mech. 177, 133–166.

Launder, B.E., Reece, G.J., Rodi, W., 1975. Progress in the development of a Reynolds-stress turbulence closure. J. Fluid Mech. 68, 537–566.

Launder, B.E., Spalding, D.B., 1974. The numerical computation of turbulent flows. Comp. Methods Appl. Mech. Eng. 3, 269–289.

Lien, F.S., Chen, W.L., Leschziner, M.A., 1996. Low-Reynolds-number eddy-viscosity modelling based on nonlinear stress–strain/vorticity relations, Third Symposium on Engineering Turbulence Modelling and Measurements, Crete.

Lien, F.S., Leschziner, M.A., 1993. A pressure-velocity solution strategy for compressible flow and its application to shock/boundary-layer interaction using second-moment turbulence closure. J. Fluids Eng. 115, 717–725.

Lien, F.S., Leschziner, M.A., 1994. A general nonorthogonal collocated finite volume algorithm for turbulent flow at all speeds incorporating second-moment turbulence-transport closure, Part 1: Computational implementation. Comput. Meth. Appl. Mech. Eng. 114, 123–148.

Obi, S., Aoki, K., Masuda, S., 1993. Experimental and computational study of turbulent separating flow in an asymmetric plane diffuse. Proceedings of the Ninth Symposium on Turbulent Shear Flows, Kyoto.

Piccin, O., Cassoudesalle, D., 1987. Etude dans la soufflerie F1 des profiles AS239 et AS240. ONERA Technical Report, PV 73/1685 AYG.

Pope, S.B., 1975. A more general effective-viscosity hypothesis. J. Fluid Mech. 72, 331–340.

Rodi, W., 1976. A new algebraic relation for calculating the Reynolds stresses. Z. Angew. Math. Mech. 56, 219–221.

Rubinstein, R., Barton, J.M., 1990. Nonlinear Reynolds stress models and the renormalisation group. Phys. Fluids A 2, 1472–1476.

Shih, T.-H., Zhu, J., Lumley, J.L., 1993. A realisable Reynolds stress algebraic equation model. NASA TM 105993.

Shih, T.-H., Liou, W.W., Shabbir, A., Yang, Z., Zhu, J., 1995. A new $k-\varepsilon$ eddy viscosity model for high Reynolds number turbulent flows. Computers Fluids 24, 227–238.

Spalart, P.R., 1988. Direct numerical simulation of a turbulent boundary layer up to $R = 1410$. J. Fluid Mech. 187, 61–98.

Speziale, C.G., 1987. On nonlinear $K-1$ and $K-\varepsilon$ models of turbulence. J. Fluid Mech. 178, 459–475.

Wilcox, D.C., 1994. Simulation of transition with a two-equation turbulence model. AIAA J. 32, 247–255.